

Single-polarization Hybrid Hollow-core Anti-resonant Fiber Designs at 2 μm

Herschel Herring, Md. Selim Habib, *Senior Member, IEEE, Senior Member, Optica*

Abstract—In this letter, to the best of our knowledge, a new type of hollow-core anti-resonant fiber (HC-ARF) design using hybrid silica/chalcogenide cladding is presented for single-polarization, high-birefringence, and endlessly single-mode operation at 2 μm wavelength. We show that the inclusion of a chalcogenide layer in the cladding allows strong suppression of x -polarization, while maintaining low propagation loss and single-mode propagation for y -polarization. The optimized HC-ARF design includes a combination of low propagation loss, high-birefringence, and polarization-extinction ratio (PER) or loss ratio of 0.02 dB/m, 1.2×10^{-4} , >550 respectively, while the loss of the x -polarization is >20 dB/m. The proposed fiber may also be coiled to small bend radii while maintaining low bend-loss of ≈ 0.01 – 0.1 dB/m, and can potentially be used as polarization filter based on the different gap separations and bend conditions.

Index Terms—Hollow-core anti-resonant fiber, high-birefringence, single-polarization, single-mode fiber.

I. INTRODUCTION

THE 2 μm wavelength is of particular interest in the field of optics and photonics due to its unique property of high absorption in water. This characteristic allows for an enormous range of optical fiber system applications such as biomarker detection, environmental observation, and molecular spectroscopy [1], [2]. High light transmission, excellent polarization control, and high-birefringence are much needed for many optical devices such as fiber sensors [3], fiber lasers [4], optical amplifiers [5], and fiber based gyroscopes [6]. Although several designs in the past have achieved high-birefringence and single-polarization in solid-core [7] and photonic band gap [8] fibers, hollow-core anti-resonant fibers (HC-ARFs) have proven to be the foremost choice because of their unique and exceptional optical guidance in air [9]. HC-ARFs guide light through inhibited-coupling between the core and cladding modes (CMs) and anti-resonant effect [10]. This mechanism provides wide transmission bandwidth [11]–[14], extremely low power overlap with cladding tubes [15], low anomalous dispersion [16] and extremely low loss [17].

Achieving high-birefringence and single-polarization using the HC-ARF structure is a relatively new concept, which was first proposed in 2016 [18]. Recently, a few high-birefringence and single-polarization HC-ARF designs have been proposed in the near-IR regime mostly at 1550 nm or 1064 nm with

different cladding arrangements and number of layers in the cladding structure [18]–[21]. High-birefringence and single-polarization were achieved either by using multiple nested resonators [18], [21] or high index materials in the cladding [19], [20]. Most recently, a four-fold [21] and six-fold [22] symmetry bi-thickness HC-ARF were experimentally reported with outstanding optical performances. For example, in [21], a phase birefringence of 2.35×10^{-5} and 9.1×10^{-5} at 1550 and 1589 nm were achieved respectively.

However, to the best of our knowledge, single-polarization, and single-mode HC-ARFs have not yet been investigated at 2 μm . In this paper, we propose a semi-nested HC-ARF design that utilizes a hybrid silica/chalcogenide cladding to attain low propagation loss, single-polarization, high-birefringence, and endlessly single-mode operation simultaneously at 2 μm .

II. FIBER GEOMETRY

The HC-ARF geometries investigated in this work are displayed in Fig. 1(a–b). Fig. 1(a) shows a semi-nested 6-tube non-touching HC-ARF architecture in which chalcogenide (As_2Se_3) tubes (orange color) are inserted into two horizontally placed silica tubes and two of the nested tubes are removed from those silica tubes to ensure low loss in one polarization state (y -polarization) and high loss for the other polarization state (x -polarization). Chalcogenide is used due to its high transmission at 2 μm . The HC-ARF has core diameter of D_c , tube diameter D , wall thickness of silica/ As_2Se_3 tubes, t_1/t_2 , nested tube ratio, d/D , and a gap separation between the outer tubes, g . Fig. 1(b) shows a regular HC-ARF design without nested tubes. In all our simulations, we choose a relatively large core diameter of $D_c = 56 \mu\text{m}$ to ensure low loss in the y -polarization. However, we optimize the silica/chalcogenide tube thickness (t_1/t_2), and gap separation, g to ensure single-polarization, single-mode, and high-birefringence. The outer diameter D is related to the core diameter D_c , wall thickness t_1 , and number to tubes N , which can be written as [23]:

$$\frac{D}{2} = \frac{\frac{D_c}{2} \sin(\frac{\pi}{N}) - \frac{g}{2} - t_1(1 - \sin(\frac{\pi}{N}))}{1 - \sin(\frac{\pi}{N})}. \quad (1)$$

III. NUMERICAL RESULTS AND DISCUSSION

The simulations were performed using fully-vectorial finite-element (FE) modeling. A perfectly-matched layer (PML) boundary was placed outside the fiber domain to accurately calculate the confinement loss. The mesh size and PML boundary conditions were chosen similar to [11], [20], [24]. The propagation loss was calculated by considering confinement

Manuscript received March XX, 2023. M. Selim Habib acknowledges partial support of this research was provided by the Woodrow W. Everett, Jr. SCEEE Development Fund in cooperation with the Southeastern Association of Electrical Engineering Department Heads.

H. Herring and M. Selim Habib are with the Department of Electrical and Computer Engineering, Florida Polytechnic University, FL-33805, USA (e-mail: mhabib@floridapoly.edu).

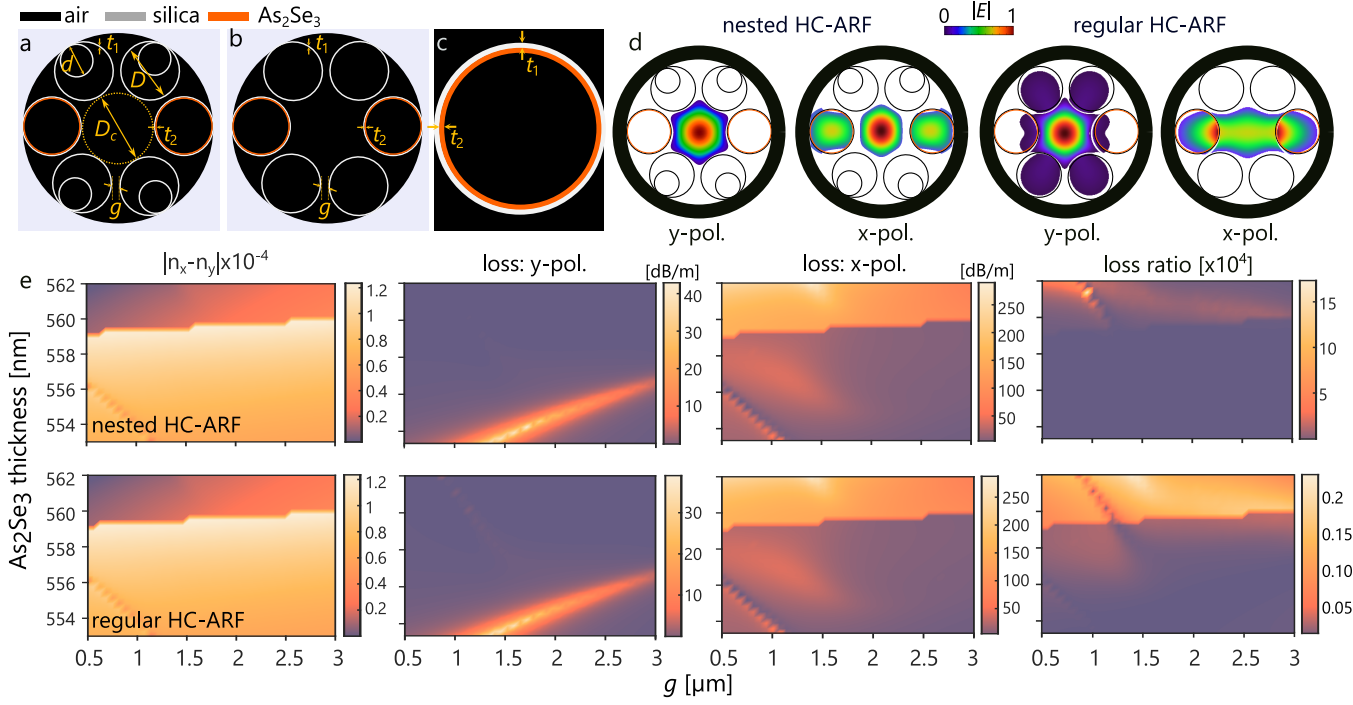


Fig. 1. HC-ARF geometries: 6-tube (a) semi-nested HC-ARF with six nested tubes and (b) regular HC-ARF in which the nested tubes are not present in the outer tubes. (c) Both fibers have a core diameter of $D_c = 56 \mu\text{m}$, $t_1/t_2 =$ wall thickness of silica/ As_2Se_3 tubes, $d =$ nested tube diameter, $D =$ outer tube diameter, $g =$ separation between the outer tubes. (d) Normalized mode-field profiles of both polarizations for nested and regular HC-ARF at $2 \mu\text{m}$. The color bar shows the intensity distributions in a linear scale. The mode-field profile (y-pol.) of nested HC-ARF is more confined to the core compared to the regular HC-ARF. (e) The FE- simulated results of birefringence: $|n_x - n_y|$, propagation loss in dB/m of y- and x- polarizations, and PER or loss ratio of both polarizations. Top panel: nested HC-ARF, and bottom panel: regular HC-ARF. The simulations were performed at $2 \mu\text{m}$. To plot the 2D surface plots, gap separation, g , and As_2Se_3 wall thickness, t_2 were scanned with 30 and 40 data points respectively and between the data points are interpolated.

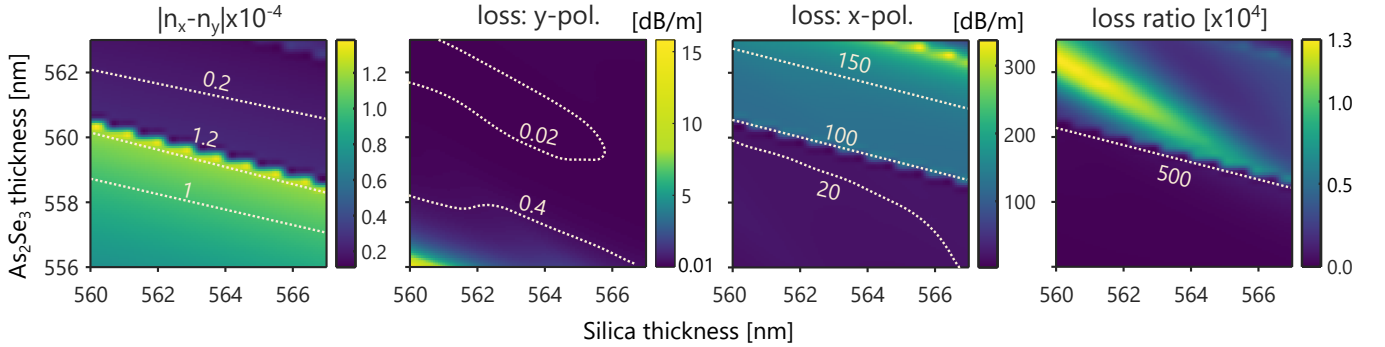


Fig. 2. The FE- simulated results of birefringence: $|n_x - n_y|$, propagation loss of y- and x- polarizations, and loss ratio of both polarizations as a function of As_2Se_3 thickness, t_2 with different values of silica thickness, t_1 . The HC-ARF has core diameter, $D_c = 56 \mu\text{m}$, normalized tube ratio, $d/D = 0.5$, and gap separation, $g = 2 \mu\text{m}$. The simulations were performed at $2 \mu\text{m}$. Silica wall thickness, t_1 , and As_2Se_3 wall thickness, t_2 were scanned with 25 and 30 data points respectively and between the data points are interpolated.

loss, effective material loss [24], and surface scattering loss (SSL) [11], [25].

A. Optimization of gap separation and As_2Se_3 wall thickness

We started our investigations towards achieving high-birefringence, single-mode, and single-polarization by optimizing the gap separation, g , and the chalcogenide (As_2Se_3) wall thickness, t_2 for a fixed the core diameter, $D_c = 56 \mu\text{m}$, silica wall thickness, $t_1 = 560 \text{ nm}$, and normalized nested tube ratio, $d/D = 0.5$. The desired properties of low loss, single-polarization, and high-birefringence are highly dependent on

these two parameters. In particular, the effect of g is critical to examine since it heavily influences how the fundamental-mode (FM) of one polarization is guided in the core while that of the other polarization spreads to the cladding. Fig. 1(d) shows the mode-field profiles of both nested and regular HC-ARFs in which it can be seen that the light of y-polarization is almost entirely guided in the core, while the light of x-polarization spreads more towards the As_2Se_3 cladding. It is also clear that there is enhanced performance with the nested HC-ARF compared to regular HC-ARF as more of the light is well guided in the core and weakly leaks towards the cladding.

The FE-simulated results for semi-nested and regular HC-ARF are shown in Fig. 1(e). From the 2D surface plots, we can see that there is low loss for y -polarization, high loss for x -polarization, high-birefringence, and high loss ratio around the region where $g = 2 \mu\text{m}$ and $t_2 = 559 \text{ nm}$. The graphical patterns for the semi-nested and regular HC-ARF are similar in regards to birefringence and the loss of both polarizations, however the semi-nested structure displays a much higher loss ratio. Numerically, the semi-nested structure also shows significantly lower loss of the y -polarization with a minimum FM loss of $\approx 0.0011 \text{ dB/m}$ comparing to that of the regular structure at $\approx 0.05 \text{ dB/m}$. It is also evident that the ideal range is more highly impacted by the value of the As_2Se_3 wall thickness, since there is a visible boundary near $t_2 = 559 \text{ nm}$ where the birefringence drops greatly from $>1.23 \times 10^{-4}$ to $<0.27 \times 10^{-4}$. For both semi-nested and regular HC-ARFs, the maximum possible loss of x -polarization, birefringence, and loss ratio as well as the minimum loss of the y -polarization do not all occur at the same values of g and t_2 . For example, the semi-nested structure's best values are 290 dB/m , $>1.23 \times 10^{-4}$, $>1.7 \times 10^5$, and $\approx 1 \text{ dB/km}$ respectively, and all occurring for different values of g and t_2 . The optimal region where high-birefringence of $>1.0 \times 10^{-4}$ is achieved while maintaining an FM loss of the y -polarization of $<0.05 \text{ dB/m}$ is highly sensitive, and occurs where $g = 2 \mu\text{m}$ and $559 \text{ nm} < t_2 < 559.5 \text{ nm}$. A polarization-extinction ratio (PER) or loss ratio of >550 is shown in this region as well. Values near this t_2 range were chosen for analysis in further sections with the anticipation that high-birefringence, low loss, and single-mode operation could be enhanced with additional parameter tuning.

B. Optimization of silica/ As_2Se_3 wall thickness (t_1/t_2)

In this section, we optimized the wall thicknesses of silica/ As_2Se_3 , while fixing our gap separation, $g = 2 \mu\text{m}$ as found in the previous section. Here, we maintained the fixed core diameter and normalized nested tube ratio of $D_c = 56 \mu\text{m}$ and $d/D = 0.5$ respectively. From the results of the 2D contour plots seen in Fig. 2, we can see that the wall thicknesses are crucial to achieving low loss, high-birefringence, and single-polarization. As mentioned previously, we chose the value of $g = 2 \mu\text{m}$ with the anticipation that further parameter tuning could lead to enhanced birefringence. From the simulated results of the silica/ As_2Se_3 sweep, high-birefringence of $>1.20 \times 10^{-4}$ was achieved in the region where $t_1 = 564 \text{ nm}$ and $t_2 = 559 \text{ nm}$. At these values, the FM loss of the y -polarization can be made as low as 0.02 dB/m while the loss of the x -polarization is $>20 \text{ dB/m}$. The loss ratio is in the range of 578-970 here as well. Again, the birefringence is highly sensitive to changes in the wall thickness of As_2Se_3 and a sharp drop can be seen once it exceeds 559 nm . These results demonstrate that by sufficient tuning of the silica thickness t_1 , we are able to enhance the properties of low loss, high-birefringence, and single-polarization. By doing so, we were able to increase high-birefringence from $>1.0 \times 10^{-4}$ to $>1.2 \times 10^{-4}$ and loss ratio from >400 to >550 while reducing the FM loss of the y -polarization from $<0.05 \text{ dB/m}$ to $<0.03 \text{ dB/m}$.

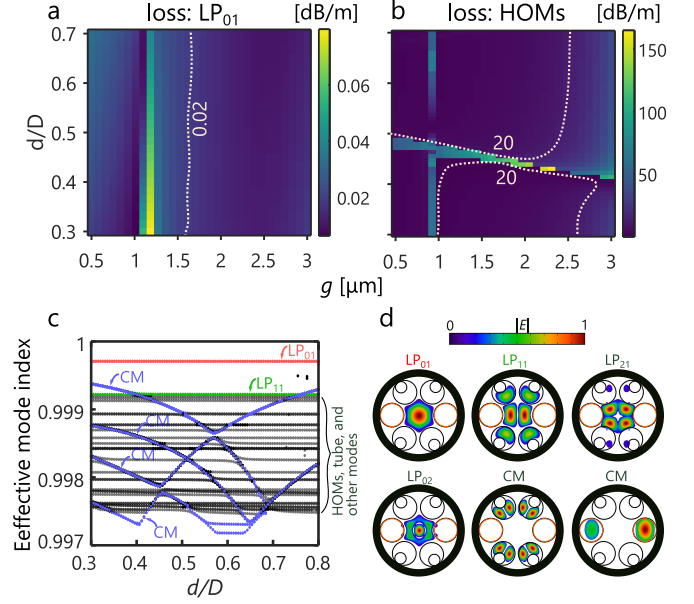


Fig. 3. The FE- simulated propagation loss of y -polarization for (a) LP_{01} -mode and (b) HOMs for varying values of d/D and gap separation, g . Results were scanned with 50 and 30 data points respectively and between the data points are interpolated. Effect of changing normalized nested tube ratio, d/D on (c) Effective mode index with a core diameter, $D_c = 56 \mu\text{m}$, $t_1/t_2 = 564/559 \text{ nm}$, and gap separation, $g = 2 \mu\text{m}$. The normalized tube ratio, d/D were scanned from 0.3 to 0.8 by simulating 50 modes at $2 \mu\text{m}$. (d) The electric field intensities of the first four core-guided modes and CMs are shown for $d/D \approx 0.42$ and $g = 2 \mu\text{m}$ on a linear color scale.

C. Single-mode operation and higher-order mode suppression

Following the examination of the low loss, high-birefringence, and single-polarization, the effectively single-mode operation and the suppression of the higher-order modes (HOMs) is demonstrated by optimization of the gap separation, g , and the nested tube ratio, d/D . The FE- simulated results for this are shown in Fig. 3, where we can easily see that there is a large region where the loss of the FM is very low ($<0.02 \text{ dB/m}$) while the loss of the HOMs is high ($>20 \text{ dB/m}$). It is also important to note that FM loss is more heavily influenced by changes in g compared to changes in d/D . However, d/D has a significant impact on the loss of the HOMs. The region of highest loss of the HOMs becomes narrow for the range $1 \mu\text{m} < g < 2.5 \mu\text{m}$, where the value of d/D must be precise in order to obtain effectively single-mode operation. The coupling between the core-guided HOMs and CMs is shown in Fig. 3(c-d). The effective mode index of the FM-like mode (red dotted line) remains unchanged as a function of d/D , avoiding any phase matching with CMs. This mechanism confirms low loss guidance. However, the effective index of HOMs strongly couple with CMs and tube modes at various values of d/D (also see Fig. 3(d), ensuring high loss for HOMs, thus confirming effective single-mode operation.

D. Bend loss analysis

Lastly, we examined the bend loss using [11] of semi-nested HC-ARF for a range of bend radii R_b of $5 - 10 \text{ cm}$ for different $g = \{2, 3, 4\} \mu\text{m}$, fixed core diameter $D_c = 56 \mu\text{m}$, $t_1/t_2 =$

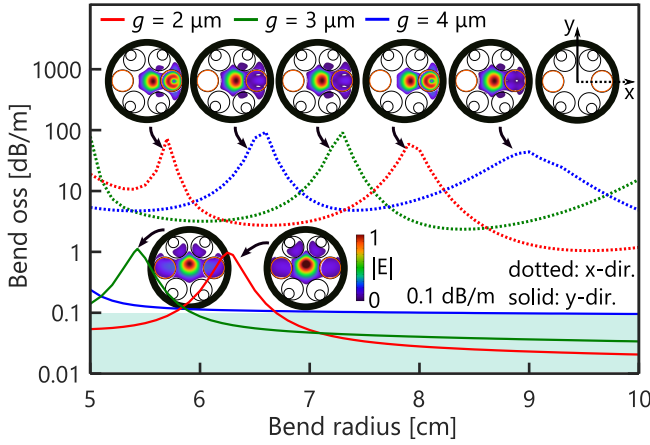


Fig. 4. Calculated bend loss of y-polarization vs. bend radius from 5 cm to 10 cm in steps of 0.1 cm for different gap separations for x- and y-bend directions. The HC-ARF has core diameter, $D_c = 56 \mu\text{m}$, silica/ As_2Se_3 wall thickness, $t_1/t_2 = 564/559 \text{ nm}$, gap separation, $d/D = 0.65$, and $g = 2 \mu\text{m}$ (red), $3 \mu\text{m}$ (green), and $4 \mu\text{m}$ (blue). The simulations were performed at $2 \mu\text{m}$. The high loss peaks can be used for polarization filters. Inset: the electric field intensities on a linear color scale are shown for different bend radii.

564/559 nm, and normalized nested tube ratio, $d/D = 0.65$. The bend loss of x-direction is much higher than y-direction and has strong light coupling to the tube modes as expected due to the missing nested tubes in the x-directions. The strong coupling between the core modes and tubes modes occur at different bend radii and the coupling shifts for different g values. This phenomenon is interesting because it indicates that the fiber can be used as a polarization filter at those gap separations and bend conditions as displayed in Fig. 4.

ACKNOWLEDGMENT

The authors would like to thank Dr. Rodrigo Amezcua-Correa for providing high performance computational support.

IV. CONCLUSION

In conclusion, we present a novel HC-ARF architecture that has been developed and validated to have single-polarization, high-birefringence, and single-mode operation characteristics at the $2 \mu\text{m}$ wavelength. Through extensive fiber parameter optimizations based on regular and semi-nested hybrid silica/chalcogenide HC-ARF structures, we demonstrated that the semi-nested geometry has better performance compared to regular HC-ARF. We also found a favorable range of the gap separation and chalcogenide wall thickness. From there, we were able to tune the silica thickness to obtain enhanced low loss, high-birefringence, and polarization-extinction ratio of 0.02 dB/m, 1.2×10^{-4} , and >550 respectively. Furthermore, effectively single-mode operation was achieved by suitably choosing the nested tube ratio, d/D . We found that the loss of the HOMs could be made as high as 20 dB/m while the loss of the FM was $<0.02 \text{ dB/m}$ for a large range of g and d/D values. Finally, we investigated the effect of changing the bend radius in both x and y-directions. The strong coupling between the core-guided modes and CMs lead to an interesting phenomenon through which the proposed fiber can be used as polarization filter. The exceptional polarization, low propagation loss, and single-mode properties presented in this work will pave the way toward practical applications at the highly appealing $2 \mu\text{m}$ wavelength.

REFERENCES

- [1] K. Scholle, S. Lamrini, P. Koopmann, and P. Fuhrberg, "2 μm laser sources and their possible applications," in *Frontiers in Guided Wave Optics and Optoelectronics*. Rijeka: IntechOpen, 2010.
- [2] S. B. Mirov, *et al.*, "Progress in mid-IR lasers based on Cr and Fe-doped ii-vi chalcogenides," *IEEE Journal of Selected Topics in Quantum Electronics*, vol. 21, no. 1, pp. 292–310, 2015.
- [3] S. Chen, *et al.*, "Local electric field enhancement and polarization effects in a surface-enhanced raman scattering fiber sensor with chessboard nanostructure," *Optics Express*, vol. 16, no. 17, pp. 13 016–13 023, 2008.
- [4] J. T. Lin and W. A. Gambling, "Polarisation effects in fibre lasers: phenomena, theory and applications," in *IEE Colloquium on Polarisation Effects in Optical Switching and Routing Systems*. IET, 1990, pp. 10–1.
- [5] X. Peng and L. Dong, "Fundamental-mode operation in polarization-maintaining ytterbium-doped fiber with an effective area of $1400 \mu\text{m}^2$," *Optics Letters*, vol. 32, no. 4, pp. 358–360, 2007.
- [6] M. A. Terrel, M. J. Dignonnet, and S. Fan, "Resonant fiber optic gyroscope using an air-core fiber," *Journal of Lightwave Technology*, vol. 30, no. 7, pp. 931–937, 2011.
- [7] T. Hosaka, *et al.*, "Low-loss single polarisation fibres with asymmetrical strain birefringence," *Electronics Letters*, vol. 17, no. 15, pp. 530–531, 1981.
- [8] J. M. Fini, *et al.*, "Polarization maintaining single-mode low-loss hollow-core fibres," *Nature Communications*, vol. 5, no. 1, pp. 1–7, 2014.
- [9] H. Sakr, *et al.*, "Hollow core optical fibres with comparable attenuation to silica fibres between 600 and 1100 nm," *Nature communications*, vol. 11, no. 1, pp. 1–10, 2020.
- [10] F. Couny, *et al.*, "Generation and photonic guidance of multi-octave optical-frequency combs," *Science*, vol. 318, no. 5853, pp. 1118–1121, 2007.
- [11] F. Poletti, "Nested antiresonant nodeless hollow core fiber," *Optics Express*, vol. 22, no. 20, pp. 23 807–23 828, 2014.
- [12] M. S. Habib, O. Bang, and M. Bache, "Low-loss hollow-core silica fibers with adjacent nested anti-resonant tubes," *Optics Express*, vol. 23, no. 13, pp. 17 394–17 406, 2015.
- [13] M. S. Habib *et al.*, "Low-loss single-mode hollow-core fiber with anisotropic anti-resonant elements," *Optics Express*, vol. 24, no. 8, pp. 8429–8436, 2016.
- [14] A. I. Adamu, *et al.*, "Deep-UV to mid-IR supercontinuum generation driven by mid-IR ultrashort pulses in a gas-filled hollow-core fiber," *Scientific Reports*, vol. 9, no. 1, pp. 1–9, 2019.
- [15] M. Michieletto, *et al.*, "Hollow-core fibers for high power pulse delivery," *Optics Express*, vol. 24, no. 7, pp. 7103–7119, 2016.
- [16] H. Sakr, *et al.*, "Interband short reach data transmission in ultrawide bandwidth hollow core fiber," *Journal of Lightwave Technology*, vol. 38, no. 1, pp. 159–165, 2020.
- [17] G. T. Jasion, *et al.*, "0.174 dB/km hollow core double nested antiresonant nodeless fiber (dnanf)," in *2022 Optical Fiber Communications Conference and Exhibition (OFC)*. IEEE, 2022, pp. 1–3.
- [18] S. A. Mousavi, S. R. Sandoghchi, D. J. Richardson, and F. Poletti, "Broadband high birefringence and polarizing hollow core antiresonant fibers," *Optics Express*, vol. 24, no. 20, pp. 22 943–22 958, 2016.
- [19] S. Yan, *et al.*, "A new method to achieve single-polarization guidance in hollow-core negative-curvature fibers," *IEEE Access*, vol. 8, pp. 53 419–53 426, 2020.
- [20] M. S. Habib, A. Adamu, C. Markos, and R. Amezcua-Correa, "Enhanced birefringence in conventional and hybrid anti-resonant hollow-core fibers," *Optics Express*, vol. 29, no. 8, pp. 12 516–12 530, 2021.
- [21] Y.-f. Hong, *et al.*, "Highly birefringent anti-resonant hollow-core fiber with a bi-thickness fourfold semi-tube structure," *Laser & Photonics Reviews*, vol. 16, no. 5, p. 2100365, 2022.
- [22] S. Yerolatsitis, *et al.*, "Birefringent anti-resonant hollow-core fiber," *Journal of Lightwave Technology*, vol. 38, no. 18, pp. 5157–5162, 2020.
- [23] C. Wei, R. J. Weiblen, C. R. Menyuk, and J. Hu, "Negative curvature fibers," *Advances in Optics and Photonics*, vol. 9, no. 3, pp. 504–561, 2017.
- [24] M. S. Habib, *et al.*, "Single-mode, low loss hollow-core anti-resonant fiber designs," *Optics Express*, vol. 27, no. 4, pp. 3824–3836, 2019.
- [25] P. Roberts, *et al.*, "Ultimate low loss of hollow-core photonic crystal fibres," *Optics Express*, vol. 13, no. 1, pp. 236–244, 2005.